

**Carbon dioxide flow and interactions in a high rank coal
Permeability evolution and reversibility of reactive processes**

Hadi Mosleh, Mojgan; Turner, Matthew; Sedighi, Majid; Vardon, Philip J.

DOI

[10.1016/j.ijggc.2018.01.002](https://doi.org/10.1016/j.ijggc.2018.01.002)

Publication date

2018

Document Version

Accepted author manuscript

Published in

International Journal of Greenhouse Gas Control

Citation (APA)

Hadi Mosleh, M., Turner, M., Sedighi, M., & Vardon, P. J. (2018). Carbon dioxide flow and interactions in a high rank coal: Permeability evolution and reversibility of reactive processes. *International Journal of Greenhouse Gas Control*, 70, 57-67. <https://doi.org/10.1016/j.ijggc.2018.01.002>

Important note

To cite this publication, please use the final published version (if applicable).
Please check the document version above.

Copyright

Other than for strictly personal use, it is not permitted to download, forward or distribute the text or part of it, without the consent of the author(s) and/or copyright holder(s), unless the work is under an open content license such as Creative Commons.

Takedown policy

Please contact us and provide details if you believe this document breaches copyrights.
We will remove access to the work immediately and investigate your claim.

Carbon dioxide flow and interactions in a high rank coal: Permeability evolution and reversibility of reactive processes

Mojgan Hadi Mosleh^{1,2*}, Matthew Turner^{1,3}, Majid Sedighi^{1,2}, and Philip J. Vardon^{1,4}

¹ Geoenvironmental Research Centre, School of Engineering, Cardiff University, Newport Road, Cardiff, CF24 3AA, UK

² School of Mechanical, Aerospace and Civil Engineering, The University of Manchester, Manchester, M13 9PL, UK

³ IHS Global Limited, Enterprise House, Cirencester Road, Tetbury, GL8 8RX, UK

⁴ Section of Geo-Engineering, Faculty of Civil Engineering and Geosciences, Delft University of Technology, 2600 GA, Delft, The Netherlands

* Corresponding author (email: mojgan.hadimosleh@manchester.ac.uk)

Abstract

Uncertainties exist on the efficiency of CO₂ injection and storage in deep unminable coal seams due to potential reduction in the permeability of coal that is induced by CO₂ adsorption into the coal matrix. In addition, there is a limited knowledge about the stability of CO₂ stored in coal due to changes in gas partial pressure caused by potential leakage. This paper presents an experimental study on permeability evolution in a high rank coal from South Wales coalfield due to interaction with different types of gases. The reversibility of the processes and stability of the stored CO₂ in coal are investigated via a series of core flooding experiments in a bespoke triaxial flooding setup. A comprehensive and new set of high-resolution data on the permeability evolution of anthracite coal is presented

The results show a considerable reduction of permeability above 1.5 MPa CO₂ pressure that is correlated with the coal matrix swelling induced by CO₂ adsorption. Notably studied in this work, the chemically-induced strain due to gas sorption into coal, that has been isolated and quantified from the mechanically-induced strain as a result of changes in effective stress conditions. The results of post-CO₂ core flooding tests using helium (He), nitrogen (N₂) and methane (CH₄) demonstrated a degree of

31 restoration of the initial permeability. The injection of N₂ showed no significant changes in the coal
32 permeability and reversibility of matrix swelling. The initial permeability of the coal sample was
33 partially restored after replacing N₂ by CH₄. Observation of permeability evolution indicates that the
34 stored CO₂ has remained stable in coal under the conditions of the experiments.

35 **Keywords:** carbon sequestration, anthracite coal, core flooding, permeability, matrix swelling, CO₂
36 adsorption, South Wales coalfield.

37

38 1. Introduction

39 Emerging interest in deep subsurface energy applications related to geological carbon sequestration
40 has highlighted the importance of an in-depth understanding of the complex physical and chemical
41 phenomena that can occur during gas-rock interactions. Among those are the processes related to gas
42 flow in coal, which are relevant to applications such as CO₂ sequestration in unminable coal seams
43 and coalbed methane recovery. Complex and coupled physical, chemical and mechanical processes
44 can occur during the flow of gas species in coal, affecting the key flow property of the coal, *i.e.*
45 permeability. This is highlighted for the case of CO₂ interaction with coal due to the chemical and
46 physical changes in the coal microstructure during adsorption and desorption (White et al., 2005)

47 It has been shown that the permeability of coal to gas species is dependent on several factors,
48 including cleat and fracture systems (Harpalani and Chen, 1997; Olson et al., 2009), porosity, type of
49 gas and pressure and mechanical stresses (Somerton et al., 1975; Palmer and Mansoori, 1998; Sasaki
50 et al., 2004), fracture orientation (Laubach et al., 1998), and the effects of matrix swelling/shrinkage
51 induced by gas sorption. The permeability of coal can decrease with an increase in the effective stress
52 (*e.g.*, McKee et al., 1988; Jasinge et al., 2011). An increase in the effective stress can cause
53 compression of the pore space available for gas flow, resulting in permeability reduction (Ranjith and
54 Perera, 2011). It has been shown that the uptake or release of CO₂ and CH₄ is a combination of
55 adsorption or desorption processes together with matrix swelling and shrinkage (Mazzotti et al.,
56 2009). The amount of swelling depends on a number of parameters, including the structure and
57 properties of the coal, gas composition, confining stress, pore pressure, temperature, fracture
58 geometry and moisture content (Wang et al., 2013).

59 Compared to the extensive reported studies related to the adsorption and desorption of gases in coal
60 (mostly on powdered samples), a limited number of experimental investigations have been reported
61 on gas transport and reactions in intact coal samples based on core flooding experiments. Tsotsis et al.
62 (2004) reported core flooding experiments to study the mechanisms involved in CO₂ sequestration in
63 a highly volatile bituminous coal. Mazumder and Wolf (2008) conducted core flooding experiments
64 on dry and wet coal samples from the Beringen coal mines in Belgium, the Silesian coalfield in

65 Poland, and the Tupton coalfields in the UK. Yu et al. (2008) performed gas storage and displacement
66 experiments on coal samples originated from the Jincheng and Luan mines, Qinshui basin, North
67 China. Wang et al. (2010) have reported core flooding experiments on high volatile bituminous coal
68 from the Bowen Basin, Australia, and van Hemert et al. (2012) conducted a series of gas storage and
69 recovery experiments (ECBM) on coal samples from Nottinghamshire by injecting N_2 , CO_2 and
70 mixtures of these two gases. Similarly, Connell et al. (2011) studied CH_4 displacement experiment
71 with N_2 on a coal sample from The Bowen Basin, Australia at low and high gas injection pressures up
72 to 10 MPa. Gas adsorption and desorption in the coal matrix has been shown to be an influential
73 factor in permeability evolution by inducing swelling and shrinkage in coal matrix. Massarotto et al.
74 (2007) observed permeability increases between 100 to 1200% during CH_4 desorption, compared to
75 permeability decreases of 60 to 80% during CO_2 adsorption. In a study by Harpalani and Mitra
76 (2010), the reduction of permeability to CH_4 was found to be approximately 25% of the original value,
77 whereas the permeability to CO_2 was found to be 40% less than that to CH_4 . It was reported that at
78 elevated gas pressures, the swelling increased nearly linearly with the amount of CO_2 adsorbed (van
79 Bergen et al., 2009). At pressures higher than 8 MPa, the gas adsorption continued to increase but the
80 coal matrix volume remained constant, *i.e.* no coal matrix swelling occurred (Harpalani and Mitra,
81 2010; Kelemen et al., 2006; Gensterblum et al., 2010). Harpalani and Mitra (2010) showed that the
82 volumetric strain of coal due to CO_2 or CH_4 adsorption followed a Langmuir-type model.

83 Despite extensive efforts to explore the complex and coupled phenomena involved in gas-coal
84 interactions, understanding of the processes that can occur when CO_2 is injected into the coal and
85 stability of the adsorbed gas in coal is incomplete. In particular, there is limited experimental
86 knowledge related to the behaviour of high rank coals, *i.e.* anthracite, during flow and interaction with
87 different gases. Modelling concepts have been developed in the last two decades to simulate the flow
88 of gas in fractured rock including coal (*e.g.* Shi and Durucan, 2003; Salimzadeh and Khalili, 2015;
89 Hosking, 2014) that are usually based on single or double porosity approaches. These models are
90 usually based on mechanistic approaches that require appropriate constitutive relationships (*e.g.* gas
91 permeability model) and experimental data for testing. Appropriate models/constitutive relationships

92 for coal permeability should reflect the chemo-mechanics of the carbon sequestration and/or enhanced
93 coalbed methane recovery problem that require experimental dataset for testing and evaluation.

94 The investigation presented in this paper aims to address two key phenomena related to flow of gases
95 in a high rank coal: i) the permeability evolution of coal to different gas species under a range of gas
96 pressures and stress conditions, with particular focus on the adsorption induced coal matrix swelling
97 and permeability degradation during CO₂ injection, and ii) the reversibility of reactive transport
98 processes and stability of CO₂ adsorbed in coal based on indirect observations of permeability
99 evolution. The latter has been achieved by altering the partial gas pressure in coal via a sequence of
100 core flooding experiments using different types of gases. These are important aspects related to i) the
101 efficiency of CO₂ storage and potential changes in the storage capacity due to permeability evolution,
102 and ii) the stability of stored CO₂ within the reservoir in case of any changes in gas partial pressure
103 due to potential leakage events.

104 A novel sequence of core flooding experiments has been designed and conducted in two stages
105 (Figure 1). In Stage 1, permeability evolution and deformation of the coal sample by exposure to He,
106 N₂ and CO₂ were studied for a range of gas injection pressures and confining stresses, and in Stage 2,
107 the same coal sample (after interactions with CO₂) was subjected to He, N₂, and CH₄ injections and
108 due to the reduction of CO₂ partial pressure in the cleats, changes in intrinsic permeability was used as
109 an indication of CO₂ desorption.

110 **2. Materials and methods**

111 **2.1. Triaxial core flooding setup**

112 The experimental facility developed and used consists of i) a high pressure triaxial core flooding
113 system by which the transport and deformation properties can be measured and studied, ii) a pressure
114 control system, iii) a temperature control system, and iv) the ancillary system including pure and
115 mixed gas supply and analysis units (Hadi Mosleh et al., 2017b). A schematic diagram of the
116 developed laboratory facility is presented in Figure 2.

117 The triaxial cell includes a base pedestal, a top-cap, an internal submersible load cell, and local strain
118 transducers. The core sample sits within a rubber sleeve (Figure 3a), and the gas passes through a
119 porous plate at the bottom of the sample. Then it leaves the cell through a similar arrangement at the
120 top after having passed through the test core. Two axial and one radial local strain transducers (Linear
121 Variable Differential Transformer (LVDT) from GDS Instruments) are attached to the sleeve (Figure
122 3a) in order to measure the volumetric deformation of the sample under axial and radial strain
123 conditions. In addition, a ± 0.025 mm displacement transducer with an accuracy of 0.25% has been used
124 to measure the axial displacement of the sample. A Mass Flow Meter capable of measuring high flow
125 rates up to $17 \times 10^{-6} \text{ m}^3/\text{s}$ (1L/min) was used that is capable of working under both subcritical and
126 supercritical conditions, with pressures up to 20 MPa.

127 The pressure control system includes a pressure-volume controller to control the confining pressure
128 and a high pressure regulator with a needle valve to control the gas pore pressure. Two 32 MPa in-line
129 pore pressure transducers were selected to measure the inlet and the outlet gas pressures. The
130 confining system consists of a 32 MPa pressure/volume controller with a $2 \times 10^{-4} \text{ m}^3$ oil reservoir.
131 Volume changes can be measured and displayed to $1 \times 10^{-9} \text{ m}^3$ (0.001cc). In order to provide the
132 confining pressure around the sample, silicone oil 350 (Polydimethylsiloxane), as recommended by
133 ASTM STP-977 (ASTM Standards, 1988) has been used.

134 In order to control the temperature of the testing sample and providing isothermal conditions, a
135 climate control system was installed. The system comprises four heating elements (Figure 3b) and a
136 programmable controller. Heating elements provide constant temperature around the sample from
137 ambient temperature, to up to 338K (65°C). Temperature within the sample is measured using three
138 thermocouples attached to the top, middle and bottom of the sample.

139 The ancillary system comprises two main sections, including the gas supply unit and gas analysing
140 unit. The gas supply system was designed to deliver different gases with controlled pressure and
141 temperature to the triaxial core flooding system at pressures up to 30 MPa and temperatures up to
142 338K (65°C). A Haskel air driven gas booster (model AG-62-50341) has been used to pressurise the
143 gas and a set of gas reservoirs have been used to store the pressurised gases to be used for high gas

144 demand experiments. A vacuum pump was employed to evacuate the entire system including the dead
145 volumes inside the pipes and the valves to avoid any contamination of injecting gases with the
146 residual gases from previous tests. The composition of the outflow gases can be determined using an
147 Emerson X-Stream general purpose gas analyser (standard 19"/3HU version). More details related to
148 the design and development of the experimental setup can be found in Hadi Mosleh et al. (2017b).

149 **2.2. Preparation and properties of the coal sample**

150 The coal sample used in the present study was obtained from the Six Foot seam (Carboniferous) of the
151 Unity coal mine in South Wales, UK. A series of coal characterisation analyses have been conducted
152 to determine key parameters including moisture content, ash content, and volatile matter as well as
153 elemental compositions including sulphur content and carbon content. Table 1 presents a summary of
154 the physical and chemical properties of the coal sample.

155 Large blocks of coal were collected from the 6-ft seam located at approximate depth of 550 m. The
156 70mm-diameter core samples were drilled out from the coal blocks using a coring machine and were
157 then cut into the required lengths using a diamond saw. In order to allow a uniform distribution of the
158 axial stresses to both ends of the sample and to prevent breakage of the coal samples under high stress
159 conditions, the ends of the specimens were ground and made parallel to each other using a fine sand
160 paper. The core samples were then air-dried for 24hr and wrapped in a plastic cling film. The samples
161 were stored in a refrigerator to be used for the tests.

162 **2.3. Experimental procedure and measurement method**

163 A core sample with 7 mm diameter and 120 mm length was carefully wrapped with a thick PTFE
164 (Polytetrafluoroethylene) tape before placing in a silicon rubber sleeve. The PTFE tape was used as a
165 non-reactive material which prevents gas diffusion through the rubber membrane into the silicone oil
166 as well as protecting the membrane from any sharp edges that may remain on the coal surface. A 1.5
167 mm thick blue silicone rubber has been used as the membrane (Figure 3a). The displacement
168 transducers, two axial and one radial, and the thermocouples were then attached to the sample (Figure
169 3a). Top cap was placed on the base pedestal and the cell was filled with the silicone oil (Figure 3b).

170 The temperature of the system was set to the desired value and kept constant throughout the test. It is
171 noted that under the in situ conditions, zero-strain or uniaxial strain conditions are expected, however,
172 most of the experimental investigations related to the coal permeability variations with effective stress
173 have been conducted under the non-zero strain conditions (Harpalani and Mitra, 2010), *i.e.* the coal
174 samples have been allowed to expand in both axial and radial directions. Attempts were made by
175 Harpalani and Mitra (2010) to maintain zero-strain conditions during a CO₂ core flooding experiment,
176 however the excess stress required maintaining this condition was very large, resulting in sample
177 failure.

178 A confining pressure of 1 MPa was applied, and the sample was subjected to a vacuum for 24 hours.
179 After the vacuum process, the downstream valve was closed and the experimental gas was injected at
180 the upstream end. The upstream pressure was increased step by step to the desired level. Gas injection
181 at fixed pressure was continued to saturate the sample with gas. Depending on the test conditions and
182 gas type, saturation was achieved within 3 to 6 days. The condition for achieving the saturation state
183 was based on a pressure decrease less than 0.05 MPa over a 24 hr period as suggested by van Hemert
184 et al. (2012).

185 The steady-state method was then used to estimate the permeability of the coal samples. The
186 confining pressure was maintained at the desired pressure and increased step by step. The gas pressure
187 at the upstream end was fixed, at a range of pressures. The downstream pressure was constantly kept
188 at atmospheric pressure (0.1 MPa). Once the steady-state flow rate was achieved, the differential gas
189 pressures and gas flow rates were recorded and permeability of the coal sample was calculated using
190 Darcy's equation for gases (Carman, 1956):

$$k_g = \frac{2Q_0\mu_g LP_0}{A(P_{up}^2 - P_{down}^2)} \quad (1)$$

191 where, k_g is the gas permeability coefficient (m²), Q_0 is the volumetric rate of flow at reference
192 pressure (m³/s), μ_g is the gas viscosity (Pa.s), L is the sample length (m), P_0 is the reference pressure
193 (Pa), A is the cross-sectional area of the sample (m²), P_{up} is the upstream gas pressure (Pa), and P_{down}

194 is the downstream gas pressure (Pa). The viscosity of gases (μ_g) was calculated based on the
195 Sutherland formula as function of temperature (Smits and Dussauge, 2006). The results of the core
196 flooding experiments are presented and discussed in the following sections.

197 **3. Stage 1- Gas flow behaviour and permeability evolution in coal**

198 For the first stage, permeability evolution and deformation of the coal sample in response to the
199 injection of He, N₂ and CO₂ were estimated at a range of gas pressures up to 5.5 MPa and confining
200 stresses up to 6 MPa.

201 **3.1. Helium flooding experiment**

202 Figure 4a presents the results of the helium flow rates versus differential gas pressures obtained for a
203 range of gas injection pressures up to 5.5 MPa and confining pressures up to 6 MPa at 298 K. The
204 results show that despite a certain pressure gradient across the sample, no apparent flow was observed
205 and recorded at low pressures within the timescale allowed, *i.e.* 15 to 30 minutes. This effect was
206 attributed to “threshold phenomenon” (Chen et al., 2006). Accordingly a certain nonzero pressure
207 gradient (1.7 MPa/m) was required to initiate the flow.

208 The overall gas flow rate was found to increase with the increase in gas injection pressure. A
209 maximum value of $88 \times 10^{-6} \text{m}^3/\text{s}$ at approximately 5.5 MPa differential gas pressure and 6 MPa
210 confining pressure was recorded. In addition, under constant gas injection pressures, a considerable
211 decrease in the gas flow rate was observed as a result of increases in the confining pressure applied.

212 Figure 4b presents the absolute permeability of the coal sample at different gas pressures and
213 confining pressures. At constant confining pressure of 1 MPa, the absolute permeability of the coal
214 sample increased considerably due to the increase in gas injection pressure and reached a maximum
215 value of $1.35 \times 10^{-15} \text{m}^2$ (at a differential gas pressure of 0.6 MPa). The gas injection pressure was then
216 kept constant and the confining pressure was increased to 2 MPa. As a result, permeability decreased
217 by 68%. At constant gas injection pressures, an average permeability reduction of 54% was observed
218 for every 1 MPa increase in confining pressure.

219 For low permeability coals, the flow behaviour is highly dependent on the effective stress (Huy et al.,
 220 2010), and the effect of effective stress can be considerable in coal permeability changes. The average
 221 effective stress of coal subjected to a gas pressure can be expressed as (Harpalani and Chen, 1997):

$$\sigma_{eff} = P_c - \frac{P_{up} + P_{down}}{2} \quad (2)$$

222 where, σ_{eff} is the effective stress and P_c is the confining pressure.

223 Unlike water, gas is a compressible fluid and therefore its bulk density varies significantly. As the
 224 result, variation of gas pore pressure across sample length is not expected to be linear (Hadi Mosleh et
 225 al. (2017a). In this study, the analytical solution presented by Wu et al. (1998) has been used to
 226 estimate the changes in gas pore pressure across the sample at steady-state flow conditions:

$$P(x) = -b + \sqrt{b^2 + P_L^2 + 2bP_L + 2q_m\mu(L-x)/k_\infty\beta} \quad (3)$$

227 where, $P(x)$ is the gas pressure (Pa) at linear distance x (m), b is the Klinkenberg coefficient, P_L is the
 228 gas pressure at outlet boundaries of linear flow systems (Pa), q_m is the gas mass injection or pumping
 229 flux (kg/s.m^2), L is the length of linear flow systems or thickness of unsaturated zone (m), k_∞ is the
 230 absolute permeability (m^2), and β is the compressibility factor; μ viscosity (Pa.s).

231 In order to accurately estimate variation of gas pore pressure across the sample, the length of the
 232 sample was divided into 7 sections of 0.02m long, and for each section the average pore pressure was
 233 estimated using Eq. (3). Figure 4c shows estimated gas pore pressure variations across sample length,
 234 using Eq. (3), for a number of gas injection pressures. The effective stress was then calculated as the
 235 difference between confining pressure and the average gas pore pressure, at each injection pressure
 236 step.

237 By plotting the experimental results of the coal permeability to helium versus effective stress, a
 238 general trend of the coal permeability reduction can be observed as a result of an increase in the
 239 effective stress (Figure 4d). An empirical relation between the coal permeability to helium and
 240 effective stress was developed as it has been shown in Figure 4d. The exponential function
 241 demonstrates a relatively good fit with the experimental data. The exponential relationship between

242 the coal permeability and effective stress has been also reported by other researchers (Jasinge et al.,
243 2011; Chen et al., 2006; Vishal et al., 2013; McKee et al., 1988, Seidle and Huitt, 1995).

244 The permeability of coal to helium decreased sharply at lower stress conditions. This can be attributed
245 to the immediate closure of existing microfractures under low stress (Somerton et al., 1975; Durucan
246 and Edwards, 1986). Therefore, only the second section of the curve can represent the deformation
247 effects of the coal matrix under stress (Durucan and Edwards, 1986).

248 The variations of coal permeability with effective stress can be controlled by the compression of the
249 pores and fracture system at high effective stresses (Somerton et al., 1975; Durucan and Edwards,
250 1986), or as a result of both compression and microfracturing of the coal material (Durucan and
251 Edwards, 1986). The compressibility of the fracture system can change as the effective stress
252 increases (Pan et al., 2010). Therefore at higher stress conditions, the effect of effective stress on coal
253 permeability becomes less considerable. This is compatible with the observations presented in Figure
254 4d.

255 Figure 4e presents the results of the volumetric expansion of the coal sample due to the increase in gas
256 pressure under constant confining pressures. At a constant confining pressure, the increase in pore
257 pressure resulted in the decrease of the effective stress and consequently expansion of the coal
258 sample. Overall, every 0.5 MPa increase in the mean gas pressure has induced an expansion of
259 approximately 0.07% in the coal sample volume (under constant confining pressures). The total
260 expansion of the coal sample due to 2.7 MPa increase in the mean gas pore pressure was estimated to
261 be approximately 0.4%. Since helium is a non-reactive/non-adsorptive gas species, the volumetric
262 strains of the coal sample observed are purely attributed to the mechanical deformations of the coal
263 sample due to variations in effective stress, *i.e.* expansion and compression in response to the internal
264 and external forces.

265 **3.2. N₂ flooding experiment**

266 A similar experimental procedure that was performed for the helium flow measurements was repeated
267 for the N₂ flooding experiment and the permeability coefficients of the coal sample to N₂ were

268 calculated using equation (1). The variations of N₂ permeability coefficients with differential gas
269 pressures up to 5.5 MPa at several confining pressures are presented in Figure 5a. At constant gas
270 injection pressures, an average permeability reduction of 65% was observed as a result of every 1
271 MPa increment of confining pressure.

272 Figure 5b presents the variations of coal permeability to N₂ with effective stress. Similar to the helium
273 flooding results, overall permeability of the coal sample decreased with the increase in the effective
274 stress. As shown in Figure 5b, the exponential regression between the coal permeability to N₂ and
275 effective stress is relatively poor, compared to the results of first helium flooding experiments, which
276 may limit the application of the established exponential relationship.

277 The relative permeability values of the coal sample (k_r), *i.e.* $K_{(N_2)}/K_{(He)}$, were also estimated based on
278 the results of the N₂ permeability and the absolute permeability coefficients, *i.e.* He permeability, for a
279 range of gas pressures and confining pressures and presented in Figure 5c. In general, the relative
280 permeability of the coal sample to N₂ was found to be much smaller than those for helium at lower
281 pressures which can be related to the immediate closure of microfractures (Somerton et al., 1975;
282 Durucan and Edwards, 1986) and larger kinetic diameter of N₂, *i.e.* 0.36nm (Gan et al., 1972). Due to
283 the small kinetic diameter, *i.e.* 0.26 nm (Mehio et al., 2014), helium can penetrate most of the pores
284 that might not be accessible for N₂ molecules.

285 The hysteresis as a result of repeated loading and unloading cycles might have also led to the lower
286 permeability of the coal sample to N₂ (Somerton et al., 1975; Dabbous et al., 1974). Dabbous et al.
287 (1974) reported strong hysteresis due to different cleat compressibility at loading and unloading
288 cycles. Although changes in fracture system and cleat aperture has been shown to be largely
289 reversible at lower stress conditions (Wang et al., 2013), higher effective stresses can result in non-
290 reversible changes such as creating new fractures or microfractures. The relative permeability of the
291 coal sample to N₂, however, increased with an increase in gas pressure and confining pressure and
292 reached a maximum of 70% of the helium permeability at the corresponding stress condition.

293 The comparative and noncumulative volumetric expansions of the coal sample due to increases in N₂
294 pressure at constant confining pressures are presented in Figure 5d. In order to compare the effect of

295 N₂ on the volumetric strains of the coal sample with the behaviour observed during helium injection,
296 the volumetric strains from the helium flooding experiment are also included (dashed lines). The
297 results show that the amounts of coal expansion due to N₂ injection into the coal are slightly higher
298 than those obtained in the case of helium injection, especially at lower effective stress values.

299 As the effective stress increases, the expansion rate decreases that match with the results of the He
300 flooding experiment. At constant confining pressures, an average expansion rate of 0.08% was
301 observed as a result of 0.5 MPa increase in the gas pressure. Since the volumetric effect of N₂ on the
302 coal matrix due to its sorption has been found to be negligible (Hadi Mosleh, 2014), it can be assumed
303 that the volumetric deformations observed are mostly related to the mechanical deformation of the
304 coal sample.

305 The results of the volumetric strains show that at higher effective stresses, the mechanical strains of
306 the coal sample during N₂ flooding experiments are similar to those observed in the helium flooding
307 experiments. At lower effective stresses however, the differences in volumetric deformations may be
308 related to properties of the gas species (kinetic diameter) and the hysteresis and changes in the coal
309 structure as a result of loading and unloading applied during previous stages of the test. Although it
310 should be mentioned that due to complex nature of coal material, it is difficult to distinguish and
311 isolate the magnitude of the effects of different factors on the gas flow and deformation behaviour
312 observed for the coal sample. For instance, parameters such as the cleat compressibility which is often
313 considered as a constant value in a certain coal might also change with changes in effective stress
314 (Pan et al., 2010).

315 **3.3. CO₂ flooding experiment**

316 After the N₂ flooding experiment, the CO₂ flooding experiment was performed on the same coal
317 sample after applying vacuum and saturating it with CO₂ at 5 MPa gas pressure for the duration of
318 approximately 6 days. The results of permeability of the sample to CO₂ versus differential gas
319 pressures at different confining pressures are presented in Figure 6a. At constant gas pressures, every
320 1 MPa increase in the confining pressure resulted in an average permeability reduction of
321 approximately 70%. More importantly, as the injection continued, the interaction between CO₂ and

322 coal resulted in extensive coal swelling and consequently a reduction of gas flow and permeability of
323 the coal sample. At confining pressure of 6 MPa, despite a 0.5 MPa of increase in the gas pressure
324 applied the coal permeability remained almost constant. The lowest permeability value of 0.01×10^{-15}
325 m^2 was obtained at this stage.

326 Permeability decline despite the increase in pore pressure at constant confining pressures has been
327 attributed to the adsorption-induced coal swelling (Pan et al., 2010). Vishal et al. (2013) measured the
328 permeability to CO_2 of a coal sample at 5 MPa confining pressure and gas injection pressures up to 3
329 MPa. It has been reported that the permeability of the coal reduced considerably with increase in
330 injection pressure (Vishal et al., 2013). According to Wang et al. (2013), the overall change in the
331 coal permeability is a function of the mechanical response, swelling or shrinkage of the matrix and the
332 damage or fracture induced by the applied stress. The expansion of the coal matrix due to CO_2
333 adsorption leads to the closure of the cleats and fractures, which in turn reduces the permeability of
334 coal (Siriwardane et al., 2009).

335 Figure 6b presents the results of the coal permeability measurements versus effective stress. The coal
336 permeability to CO_2 decreased much faster at lower stress conditions which again can be attributed to
337 the closure of microfractures at low stresses due to the effect of CO_2 adsorbed-phase volume
338 (Somerton et al., 1975; Durucan and Edwards, 1986) combined with the matrix swelling effect
339 induced by CO_2 adsorption. As the experiment continued and gas pressure and confining pressure
340 increased, the effect of the effective stress on coal permeability became less significant (Figure 6b).
341 The matrix swelling is likely to be the dominant factor in changes of the coal permeability. In general,
342 the exponential relationship between the coal permeability to CO_2 and effective stress is found to be
343 much stronger than those observed for He and N_2 (higher coefficient of determination for the case of
344 CO_2).

345 The relative permeability of the coal sample to CO_2 , *i.e.* $K_{(\text{CO}_2)}/K_{(\text{He})}$, is presented in Figure 6c. As the
346 results show, the relative permeability of the coal sample to CO_2 at its highest was less than 30% of its
347 absolute permeability (helium permeability at corresponding pressures). Similar to the N_2 flooding
348 experiment, this can be partly attributed to the larger kinetic diameter of CO_2 compared with helium

349 as well as the hysteresis due to loading and unloading cycles. However, the effect of adsorbed-phase
350 volume on microfractures might have influenced the coal permeability even before the CO₂ flow
351 measurements, *i.e.* during saturation stage. This may explain such lower permeability of the coal
352 sample to CO₂.

353 The sharp decrease in the relative permeability of coal to CO₂ at higher effective stresses is related to
354 the effect of coal matrix swelling on cleats and fracture system at higher pressures (Jasinge et al.,
355 2011; Vishal et al., 2013; De Silva and Ranjith, 2012). The lowest relative permeability can be
356 observed at effective stress of 5.5 MPa (Figure 6c) which was found to be 5% of its initial absolute
357 permeability at corresponding stress conditions.

358 Similar behaviour for CO₂ permeability reduction with effective stress has been reported by other
359 researchers. Huy et al. (2010) conducted CO₂ core flooding experiments on different coals from
360 China, Australia, and Vietnam, to investigate the effect of effective stress on gas permeability. For
361 their experiments, the confining stress on the coal sample was increased from 1 to 6 MPa, and the
362 average gas pore pressure applied was between 0.1 and 0.7 MPa. Figure 6d shows the results of CO₂
363 permeability evolution with effective stress for the coal sample of this study (South Wales Anthracite)
364 and those studied by Huy et al. (2010). From this comparison it can be postulated that the overall gas
365 permeability behaviour of South Wales Anthracite as the result of changes in effective stress is similar
366 to those observed and reported for other types of coal. The slight differences however can be
367 attributed to various methods that might have been used to estimate the average pore pressure and the
368 effective stress values (*i.e.* Eq. 2 and Eq. 3).

369 The volumetric deformations of the coal sample due to CO₂ injection at different confining pressures
370 are presented in Figure 6e (Dashed lines represent the results of the phase 1 of helium flooding
371 experiment). The overall volumetric expansion of the coal sample during CO₂ flooding experiment
372 was much higher than those for other gases. For He and N₂ flooding experiments, it was observed that
373 although the coal sample expanded due to the increase in the pore gas pressure, the amounts of the
374 volumetric expansion at different confining pressures were almost comparable. In the case of CO₂,

375 however, this similarity is not observed and the amount of coal expansion increases more clearly
376 which can be related to the swelling effect of CO₂ adsorption on coal.

377 As higher injection pressure was applied, the difference between the volumetric strains observed in
378 the He and CO₂ flooding experiments increased considerably. At the final step of the injection, the
379 increase in the coal volume was found to be ten times more than those observed in the He flooding
380 experiment. In general, the trend of the coal permeability variation with pore pressure was found to be
381 opposite to that of the volumetric increase in coal. This behaviour can be attributed to the fact that
382 coal adsorbs more CO₂ at higher injection pressures, which leads to further swelling of the coal
383 matrix.

384 The coal sample exhibited 1.9% volume increase during the CO₂ flooding experiment. The swelling
385 effect was then quantified by subtracting the mechanical effects obtained from the phase 1 of the
386 helium flooding experiment. According to the results, the swelling effect of CO₂ in the volumetric
387 expansion of the coal is 1.5%. It should also be mentioned that the volumetric strain measured here
388 may have been underestimated for the matrix swelling because the cleat porosity may take part of the
389 displacements (Vishal et al., 2013). In addition, due to the relatively short exposure of the coal sample
390 to CO₂, the adsorption process might have not been completed and more swelling could be expected
391 for a longer exposure.

392 **4. Stage 2- Reversibility of reactive processes**

393 For the second stage, a sequence of He, N₂, and CH₄ injections was conducted on the same coal
394 sample, and the reversibility of the CO₂ sorption-induced coal swelling and permeability changes
395 investigated.

396 **4.1. Helium flooding experiment**

397 In this experiment, He was re-injected into the sample to study the potential changes in the intrinsic
398 permeability and potential reversibility of the swelling process by reducing the partial pressure of CO₂
399 in the cleat. The experimental conditions and injection pressures were similar to those performed for
400 the previous tests in Stage 1. The results of the coal permeability to helium obtained from the phase 2

401 of the helium flooding experiment are presented in Figure 7a. For comparison, the results of the phase
402 1 of helium flooding experiment (before CO₂ injection) are also included in the graph (dashed lines).

403 The results show that the coal permeability has decreased considerably as a result of coal interactions
404 with CO₂. The overall trend of the coal permeability remained almost steady throughout the test in
405 comparison to the earlier tests and did not show any significant changes with the effective stress.

406 An overall permeability reduction of 89% was observed at lower pressures. The results of relative
407 permeability of CO₂ to He (Figure 6c) suggests a larger permeability reduction (nearly 95%),
408 therefore it can be concluded that some of the coal permeability was restored due to CO₂ desorption
409 during vacuum process and helium saturation phase. At the higher gas injection pressures and
410 confining pressures, the coal permeability increased slightly and reached to a value of approximately
411 $0.07 \times 10^{-15} \text{ m}^2$, *i.e.* 75% of the initial value. The average permeability value of the coal sample was
412 increased by 14% during the phase 2 of helium injection.

413 **4.2. N₂ flooding experiment**

414 Since helium is a non-adsorptive gas, its chemical interaction with coal is very limited. Although, due
415 to an increase of helium partial pressure, CO₂ molecules can desorb first from weakly adsorbed sites,
416 it cannot replace the strongly adsorbed CO₂ molecules in coal matrix pores (micropores). With N₂,
417 however, the behaviour can be different. N₂ can be partially adsorbed to the coal and its replacement
418 with some of the adsorbed CO₂ might affect the coal swelling and permeability. In order to further
419 investigate that effect, the coal sample was subjected to the phase 2 of N₂ injections. Subsequently
420 and in order to evaluate the effect of the phase 2 of N₂ injections on changes in coal permeability and
421 swelling effects of adsorbed CO₂ (structure of the coal pore system) the phase 3 of helium flooding
422 experiment was performed. The results are presented in Figure 7b along with the results of the phase 2
423 of the He flooding experiments, *i.e.* before and after N₂ injection.

424 At confining pressures less than 2 MPa, no considerable change in the permeability of the coal sample
425 was observed. However, at higher pressures and constant confining conditions, slight increases and
426 decreases in the coal permeability was observed. Inconsistency between the results at different

427 confining pressures can be attributed to the minor differences in the experimental conditions or slight
428 changes in the coal structure during several cycles of loading and unloading. Overall, no significant
429 improvement in terms of recovery of coal permeability has been observed as a result of N₂ injection.

430 **4.3. CH₄ flooding experiment**

431 Compared to N₂, CH₄ has higher affinity to coal but still lower than that of CO₂ (Hadi Mosleh, 2014).
432 It has been also shown that its volumetric effect on coal matrix is very small, *e.g.* Battistutta et al.,
433 2010. Therefore, CH₄ was injected into the sample to study the potential displacement of the adsorbed
434 CO₂ and further improvement of the coal permeability. Figure 7c shows the results of the coal
435 permeability variations for two sets of helium flooding experiments conducted before and after the
436 CH₄ injection.

437 At lower pressures, permeability changes were found to be small. At higher pressures, however, the
438 coal permeability improved which can be partly related to the decrease in the cleat compressibility
439 due to the increase in pore pressures. On average, the permeability of the coal sample was found to
440 increase by 1.6 times as a result of CH₄ injection.

441 Although, some researchers (De Silva and Ranjith, 2012; Battistutta et al., 2010) have suggested that
442 the swelling effect is a fully reversible process, for the coal sample of this study the swelling effects
443 were found to be only partially reversed during CH₄ injection. This can be attributed to both hysteresis
444 effect and higher affinity of coal to adsorb and retain CO₂ compared with CH₄. Accordingly, the coal
445 permeability was also restored to some extent. Nonetheless, the time dependency of such processes
446 should also be taken into account when interpreting the results (Fokker and van de Meer, 2004). On
447 the other hand, the results of this investigation showed that CO₂ can be adsorbed to the coal to a great
448 extent and changes in gas partial pressure does not lead to a significant and sudden release of
449 adsorbed CO₂. Such data are crucial for assessing long-term stability of the injected CO₂ in coal
450 reservoirs, in applications such as carbon sequestration process in coal seams.

451 **5. Conclusions**

452 The results of this study have provided new insights into the interactions between various gas species
453 in a high rank coal from the South Wales coalfield. Such data-set at this level of accuracy and
454 comprehensiveness is believed to be produced for the first time for the South Wales coals. Using a
455 developed triaxial core flooding setup, a sequence of flooding tests have been designed and conducted
456 to simulate and study two key aspects related to geological sequestration of CO₂ in coal, *i.e.* efficiency
457 of the injection and stability of stored gas due to potential changes in the reservoir pressure. It was
458 shown that the coal permeability has a different level of dependency on the effective stress for
459 different gas species. Especially, the behaviour was highlighted for the case of CO₂ flooding
460 experiments in which the gas adsorption/desorption in coal demonstrated strong effect on the overall
461 permeability evolution. The effect of N₂ on permeability evolution of the coal sample was found to be
462 negligible, whereas the absolute permeability of the coal sample was found to be reduced by 95% as a
463 result of coal matrix swelling induced by CO₂ adsorption at 6 MPa confining pressure. Notably
464 studied in this work, by performing sequential core flooding experiments using non-reactive and
465 reactive gases, the chemically-induced strain due to gas sorption into coal has been isolated and
466 quantified from the mechanically-induced strain as a result of changes in effective stress conditions.
467 New dataset generated from the permeability tests are of importance for developing appropriate
468 constitutive relationships/models for permeability evolution in coal that requires reflecting the chemo-
469 mechanical interactions between CO₂ and coal in carbon sequestration and/or enhanced methane
470 recovery.

471 The results of post CO₂ core flooding experiments using He and N₂ indicated no significant changes
472 in the coal permeability and reversibility of the coal matrix swelling. The injection of CH₄ into the
473 coal sample, on the other hand, resulted in relatively considerable improvement in gas flow rates, so
474 that the initial permeability of the coal sample was restored by an average of 20%. However, the
475 initial permeability of the coal sample was not fully recovered. Based on the results of permeability
476 evolution during post CO₂ flooding tests a relative stability of the stored CO₂ in coal under the
477 experimental conditions/duration was observed

478 **Acknowledgement**

479 The financial support received from the Welsh-European Funding Organisation as part of the SEREN
480 project is gratefully acknowledged. The authors would like to thank Dr Snehasis Tripathy for his
481 helpful discussions and support. We wish to thank the GDS Instruments for their contribution for
482 construction and commissioning of laboratory equipment. Technical support from the technicians and
483 staff of the Engineering Workshop at Cardiff University is gratefully acknowledged.

484

485 **References**

- 486 ASTM Standards, 1988. *ASTM STP-977, 1988*. Advanced triaxial testing of soil and rock. In:
487 *Donaghe R.T., Chaney R.C and Silver M.L. eds.* West Conshohocken, PA: ASTM International.
- 488 Battistutta, E., van Hemert, P., Lutynski, M., Bruining, H. and Wolf, K.H. 2010. Swelling and
489 sorption experiments on methane, nitrogen and carbon dioxide on dry Selar Cornish coal.
490 *International Journal of Coal Geology*, 84(1), pp. 39-48.
- 491 Carman, P.C. 1956. *Flow of gases through porous media*. London: Butterworths.
- 492 Chen, Z., Huan, G. and Ma, Y. 2006. *Computational methods for multiphase flows in porous media*
493 *(Computational Science and Engineering)*. Philadelphia: Society for Industrial and Applied
494 Mathematics (SIAM).
- 495 Connell, L.D., Sander, R., Pan, Z., Camilleri, M. and Heryanto, D. 2011. History matching of
496 enhanced coal bed methane laboratory core flood tests. *International Journal of Coal Geology*, 87(2),
497 128-138.
- 498 Dabbous, M.K., Reznik, A.A., Taber, J.J. and Fulton, P.F. 1974. The permeability of coal to gas and
499 water. *SPE Journal*, 14(6), pp. 563-572.
- 500 De Silva, P.N.K. and Ranjith, P.G. 2012. Advanced core flooding apparatus to estimate permeability
501 and storage dynamics of CO₂ in large coal specimens. *Fuel*, 104, pp. 417-425.
- 502 Durucan, S. and Edwards, J.S. 1986. The effects of stress and fracturing on permeability of coal.
503 *Mining Science and Technology*, 3(3), pp. 205-21.
- 504 Fokker, P.A. and van de Meer, L.G.H. 2004. The injectivity of coalbed CO₂ injection wells. *Energy*,
505 29(9-10), pp. 1423-1429.
- 506 Gan, H., Nandi, S.P. and Walker, Jr.P.L. 1972. Nature of the porosity in American coals. *Fuel*, 51(4),
507 pp. 272-277.
- 508 Gensterblum, Y., van Hemert, P., Billemont, P., Battistutta, E., Busch, A., Krooss, B.M., De Weireld,
509 G. and Wolf, K.H.A.A. 2010. European inter-laboratory comparison of high pressure CO₂ sorption
510 isotherms II: Natural coals. *International Journal of Coal Geology*, 84(2), pp. 115-124.
- 511 Hadi Mosleh, M. 2014. An experimental investigation of flow and reaction processes during gas
512 storage and displacement in coal. PhD Thesis, Cardiff University.
- 513 Hadi Mosleh, M., Sedighi, M., Vardon, P.J., and Turner, M. 2017a. Efficiency of carbon dioxide
514 storage and enhanced methane recovery in a high rank coal. *Energy & Fuels*, Just Accepted
515 Manuscript, DOI: 10.1021/acs.energyfuels.7b02402.
- 516 Hadi Mosleh, M., Turner, M., Sedighi, M and Vardon, P.J. 2017b. High pressure gas flow, storage and
517 displacement in fractured rock - Experimental setup development and application. *Review of Scientific*
518 *Instruments*, 88 (015108), pp 1-14.
- 519 Harpalani, S. and Chen, G. 1997. Influence of gas production induced volumetric strain on
520 permeability of coal. *Geotechnical and Geological Engineering*, 15(4), pp. 303-25.
- 521 Harpalani, S. and Mitra, A. 2010. Impact of CO₂ injection on flow behavior of coalbed methane
522 reservoirs. *Transport in Porous Media*, 82(1), pp.141-156.
- 523 Hosking, L. 2014. Reactive transport modelling of high pressure gas flow in coal. *PhD Thesis*, Cardiff
524 University.
- 525 Huy, P.Q., Sasaki, K., Sugai, Y. and Ichikawa, S. 2010. Carbon dioxide gas permeability of coal core
526 samples and estimation of fracture aperture width. *International Journal of Coal Geology*, 83(1), pp.
527 1-10.
- 528 Jasinge, D., Ranjith, P.G. and Choi, S.K. 2011. Effects of effective stress changes on permeability of
529 latrobe valley brown coal. *Fuel*, 90(3), pp. 1292-1300.

- 530 Kelemen, S.R., Kwiatek, L.M. and Lee, A.G.K. 2006. Swelling and sorption response of selected
531 Argonne premium bituminous coals to CO₂, CH₄, and N₂. *In Proceedings of International CBM*
532 *Symposium*. Tuscaloosa, Alabama.
- 533 Laubach, S.E., Marrett, R.A., Olson, J.E. and Scott, A.R. 1998. Characteristics and origins of coal
534 cleat: A review. *International Journal of Coal Geology*, 35, pp. 175-207.
- 535 Massarotto, P., Golding, S.D., Iyer, R., Bae, J.S. and Rudolph, V. 2007. Adsorption, porosity and
536 permeability effects of CO₂ geosequestration in Permian coals. *In: International Coalbed Methane*
537 *Symposium*. Alabama, USA. CD ROM Paper 0727.
- 538 Mazumder, S. and Wolf, K. 2008. Differential swelling and permability change of coal in response to
539 CO₂ injection for ECBM. *International Journal of Coal Geology*, 74(2), pp. 123-138.
- 540 Mazzotti, M., Pini R., and Storti G. 2009. Enhanced coalbed methane recovery. *The Journal of*
541 *Supercritical Fluids*, 47(3), pp. 619-627.
- 542 McKee, C.R., Bumb, A.C. and Koenig, R.A. 1988. Stress-dependent permeability and porosity of coal
543 and other geologic formations. *SPE Formation Evaluation*, 3(1), pp. 81-91.
- 544 Mehio, N., Dai, S. and Jiang, D. 2014. Quantum mechanical basis for kinetic diameters of small
545 gaseous molecules. *The Journal of Physical Chemistry A*, 118(6), pp. 1150-1154.
- 546 Olson, J.E., Laubach, S.E. and Lander, R.H. 2009. Natural fracture characterization in tight gas
547 sandstones: integrating mechanics and diagenesis. *AAPG Bulletin*, 93 (11), pp. 1535-1549.
- 548 Palmer, I. and Mansoori, J. 1998. How permeability depends on stress and pore pressure in coal beds-
549 a new model. *SPE Reservoir Evaluation and Engineering*, 1 (6), pp.539-544.
- 550 Pan, Z., Connell, L.D. and Camilleri, M. 2010. Laboratory characterisation of coal reservoir
551 permeability for primary and enhanced coalbed methane recovery. *International Journal of Coal*
552 *Geology*, 82(3-4), pp. 252-261.
- 553 Ranjith, P.G. and Perera, M.S.A. 2011. A new triaxial apparatus to study the mechanical and fluid
554 flow aspects of carbon dioxide sequestration in geological formations. *Fuel*, 90(8), pp. 2751-2759.
- 555 Salimzadeh, S., and Khalili, N. 2015. Three-Dimensional Numerical Model for Double-Porosity
556 Media with Two Miscible Fluids Including Geomechanical Response. *International Journal of*
557 *Geomechanics*, 16(3).
- 558 Sasaki, K., Fujii, K., Yamaguchi, S., Ohga, K., Hattori, K. and Kishi, Y. 2004. CO₂ gas permeability
559 and adsorption of coal samples in consideration of CO₂ sequestration into coal seams. *Journal of the*
560 *Mining and Materials Processing Institute of Japan*, 120 (8), pp. 461-468.
- 561 Seidle, J.R. and Huitt, L.G. 1995. Experimental measurement of coal matrix shrinkage due to gas
562 desorption and implications for cleat permeability increases. *Proceedings of International Meeting on*
563 *Petroleum Engineering*. 14-17 November, Beijing, China, *SPE 30010*.
- 564 Shi, J-Q., and Durucan, S. 2003. A bidisperse pore diffusion model for methane displacement
565 desorption in coal by CO₂ injection. *Fuel*, 82(10), pp. 1219-1229.
- 566 Siriwardane, H., Haljasmaa, I., McLendon, R., Irdi, G., Soong, Y. and Bromhal, G. 2009. Influence of
567 carbon dioxide on coal permeability determined by pressure transient methods. *International Journal*
568 *of Coal Geology*, 77 (1-2), pp. 109-118.
- 569 Smits, A.J. and Dussauge, J.P. 2006. *Turbulent Shear Layers in Supersonic Flow*. 2nd ed. New York:
570 American Institute of Physics.
- 571 Somerton, W.H., Soylemezoglu, I.M. and Dudley, R.C. 1975. Effect of stress on permeability of coal.
572 *International Journal of Rock Mechanics and Mining Science and Geomechanics Abstracts*, 12(1), pp.
573 129-145.

- 574 Tsotsis, T.T., Patel, H., Najafi, B.F., Racherla, D., Knackstedt, M.A. and Sahimi, M. 2004. Overview
575 of laboratory and modelling studies of carbon dioxide sequestration in coalbeds. *Industrial and*
576 *Engineering Chemistry Research*, 43(12), pp. 2887-2901.
- 577 van Bergen, F., Spiers, C., Floor, G. and Bots, P. 2009. Strain development in unconfined coals
578 exposed to CO₂, CH₄ and Ar: Effect of moisture. *International Journal of Coal Geology*, 77(1-2), pp.
579 43-53.
- 580 van Hemert, P., Wolf, K.A.A. and Rudolph, E.S.J. 2012. Output gas stream composition from
581 methane saturated coal during injection of nitrogen, carbon dioxide, a nitrogen-carbon dioxide
582 mixture and a hydrogen-carbon dioxide mixture. *International Journal of Coal Geology*, 89, pp. 108-
583 113.
- 584 Vishal, V., Ranjith, P.G. and Singh, T.N. 2013. CO₂ permeability of Indian bituminous coals:
585 Implications for carbon sequestration. *International Journal of Coal Geology*, 105, pp. 36-47.
- 586 Wang, G.X., Wei, X.R., Wang, K., Massarotto, P. and Rudolph, V. 2010. Sorption-induced
587 swelling/shrinkage and permeability of coal under stressed adsorption/desorption conditions.
588 *International Journal of Coal Geology*, 83(1), pp. 46-54.
- 589 Wang, S., Elsworth, D. and Liu, J. 2013. Permeability evolution during progressive deformation of
590 intact coal and implications for instability in underground coal seams. *International Journal of Rock*
591 *Mechanics and Mining Sciences*, 58(1), pp. 34-45.
- 592 White, C.M., Smith, D.H., Jones, K.L., Goodman, A.L., Jikich, S.A., LaCount, R.B., DuBose, S.B.,
593 Ozdemir, E., Morsi, B.I. and Schroeder, K.T. 2005. Sequestration of carbon dioxide in coal with
594 enhanced coalbed methane recovery- A review. *Energy and Fuel*, 19(3), pp. 659-724.
- 595 Wu, Y-S., Pruess, K. and Persoff, P. (1998). Gas flow in porous media with Klinkenberg effects.
596 *Transport in Porous Media*, 32, 117-137.
- 597 Yu, H., Zhou, L., Guo, W., Cheng, J. and Hu, Q. 2008. Predictions of the adsorption equilibrium of
598 methane/carbon dioxide binary gas on coals using Langmuir and ideal adsorbed solution theory under
599 feed gas conditions. *International Journal of Coal Geology*, 73(2), pp. 115-129.

Table 1. Physical and chemical properties of the coal sample.

Moisture (%)	1.19	Carbon (%)	86.42
Sample diameter (mm)	7	Volatile matter (%)	9.56
Sample length (mm)	120	Fixed carbon (%)	84.39
Bulk density (kg/m ³)	1495	Sulphur (%)	0.79
Porosity (-)	0.05	Ash (%)	4.85

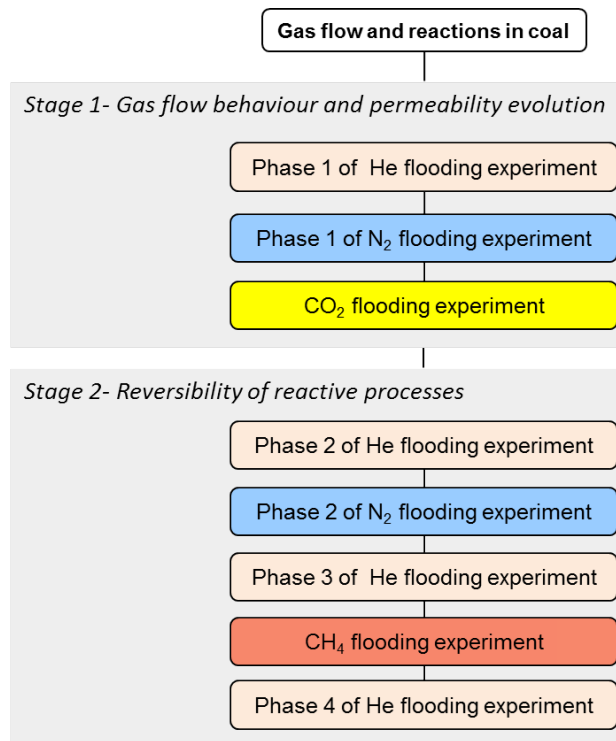


Figure 1. The flow diagram of the experimental studies on gas flow behaviour in coal and permeability evolution.

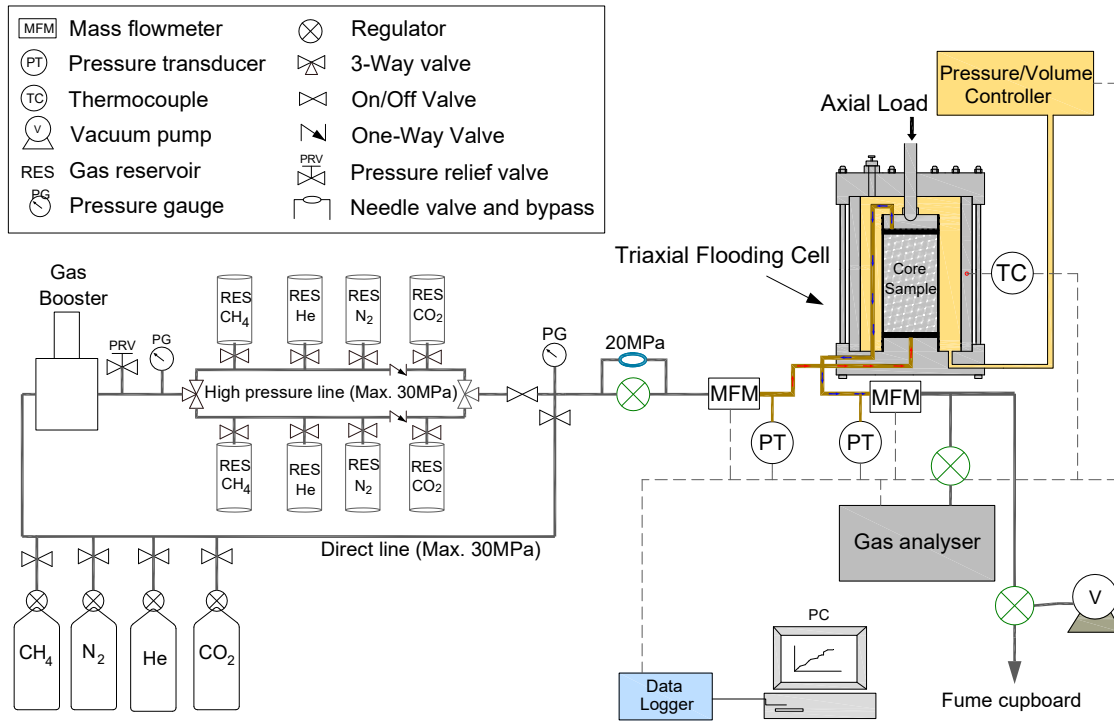


Figure 2. A schematic diagram of the developed laboratory facility (Hadi Mosleh et al., 2017a).

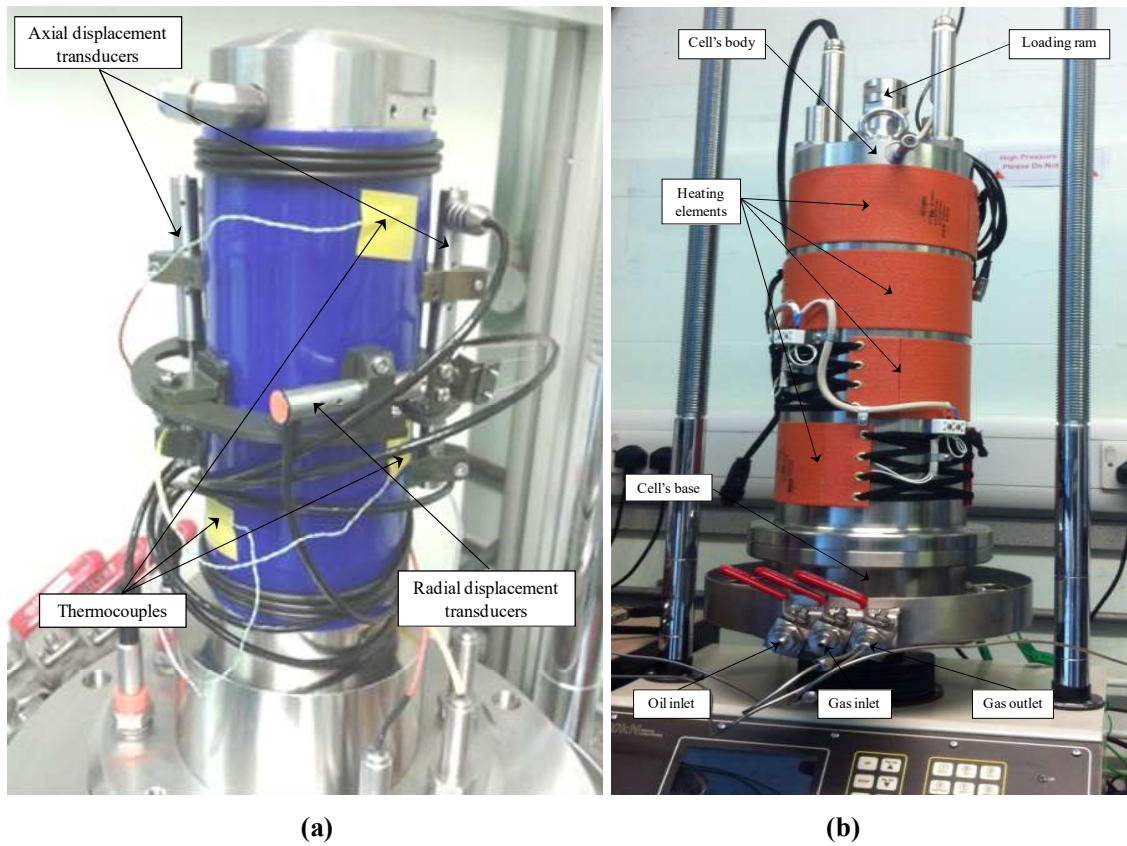


Figure 3. Triaxial core flooding cell developed and used: (a) Displacement transducers and thermocouples attached to the sample, and (b) The top cap with the heating elements, mounted on the load frame (Hadi Mosleh 2014).

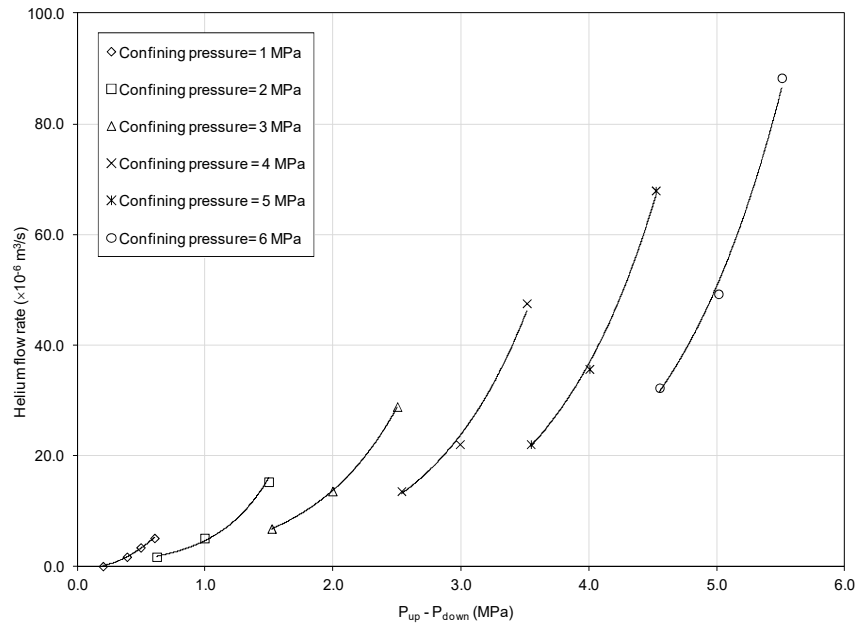


Figure 4a. Variations of helium flow rates versus differential gas pressure between the upstream and downstream at various confining pressures (T=298K).

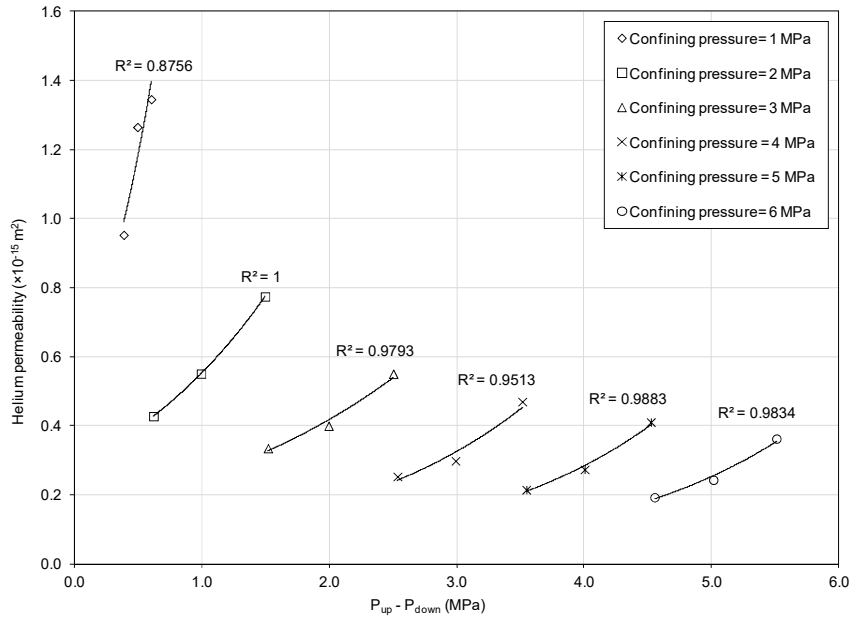


Figure 4b. Variations of absolute permeability of the coal sample to helium versus differential gas pressure between upstream and downstream at various confining pressures (T=298K).

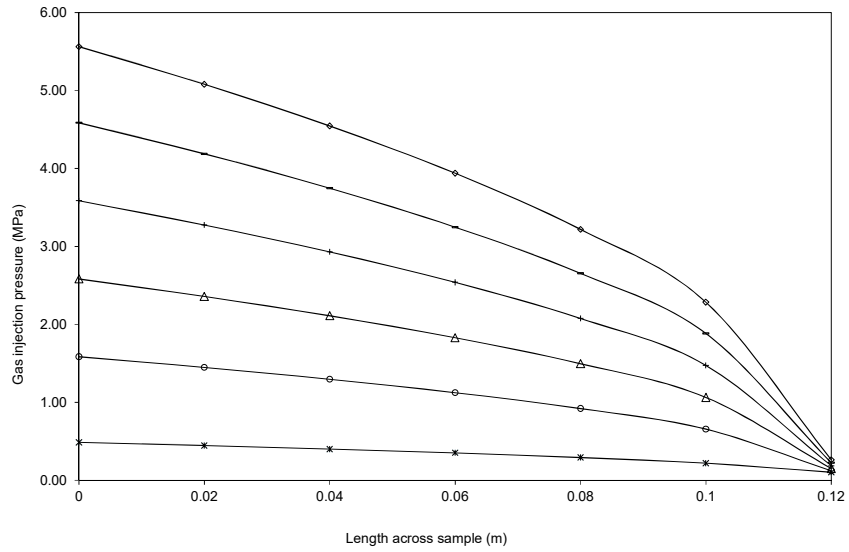


Figure 4c. Variation of gas pore pressure across sample length.

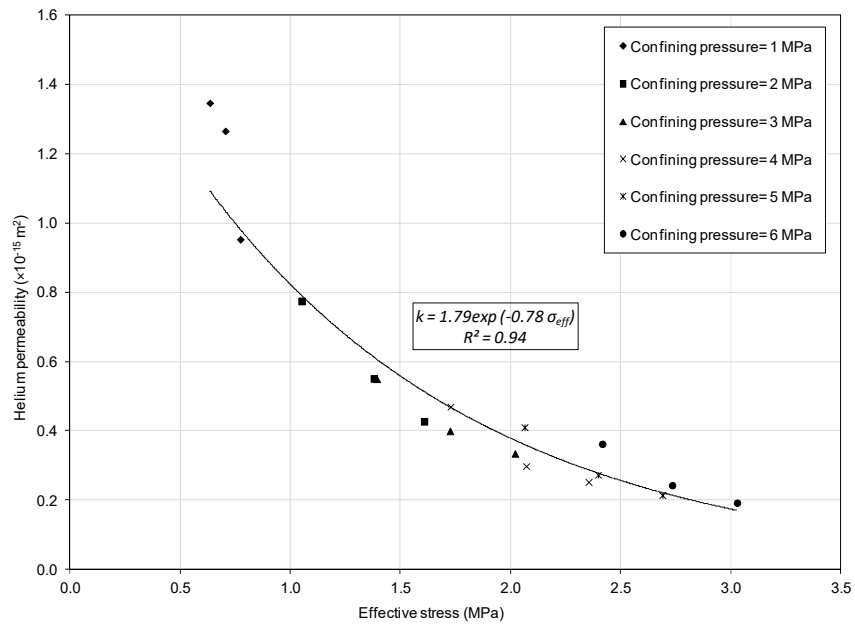


Figure 4d. The relationship between coal permeability to helium and effective stress (T=298K).

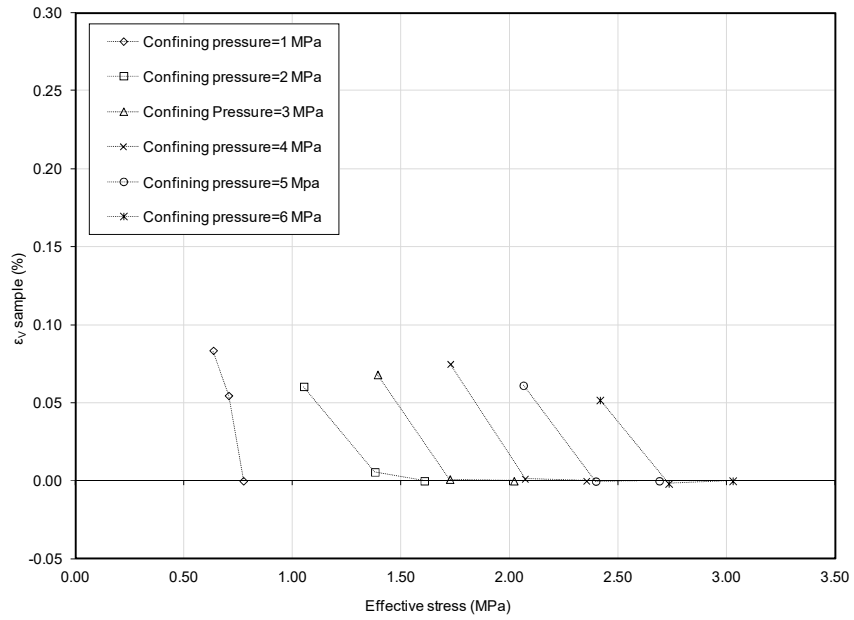


Figure 4e. Variations of the volumetric expansion of the coal sample versus effective stress due to the increase in helium pressure at constant confining pressures (T=298K).

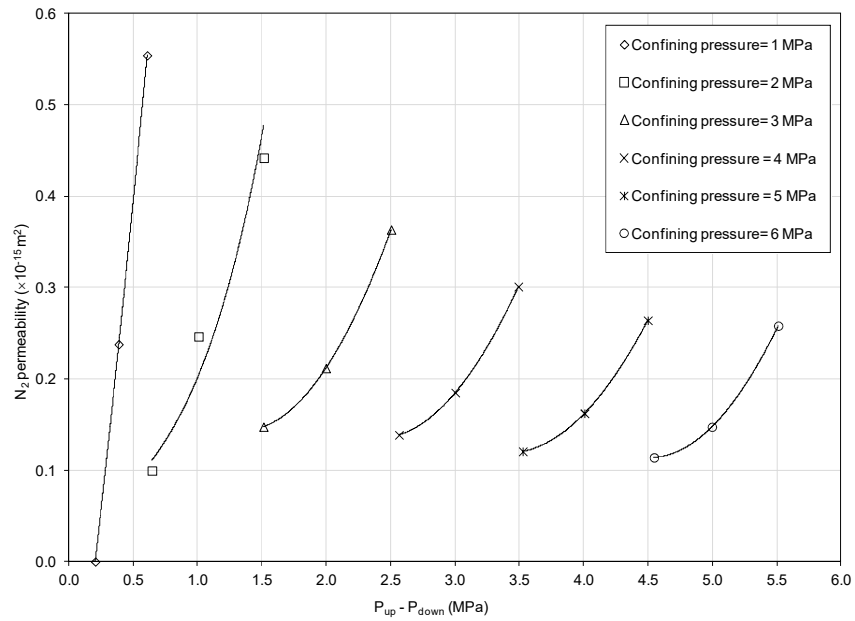


Figure 5a. Variations of permeability of the coal sample to N_2 versus differential gas pressure at various confining pressures (T=298K).

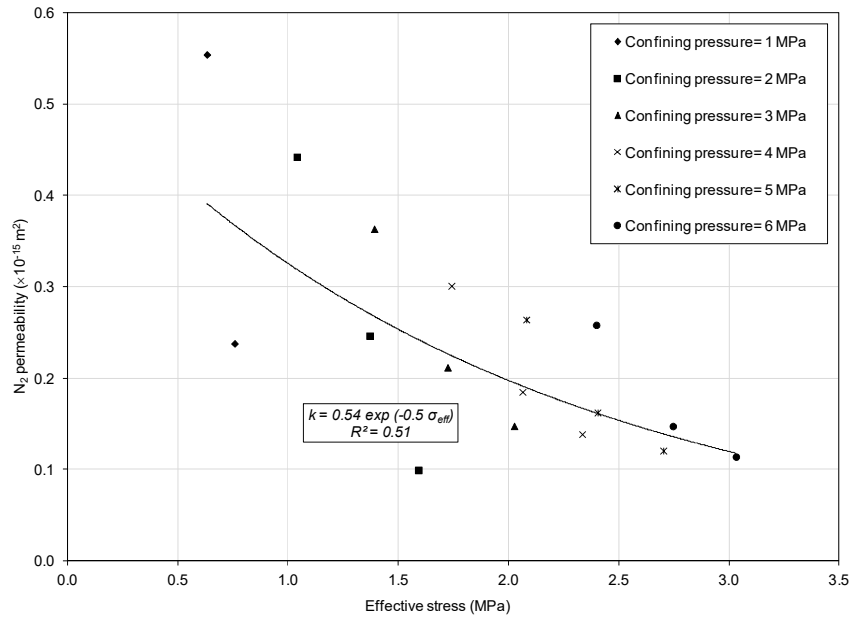


Figure 5b. The relationship between permeability of coal to N_2 and effective stress ($T=298\text{K}$).

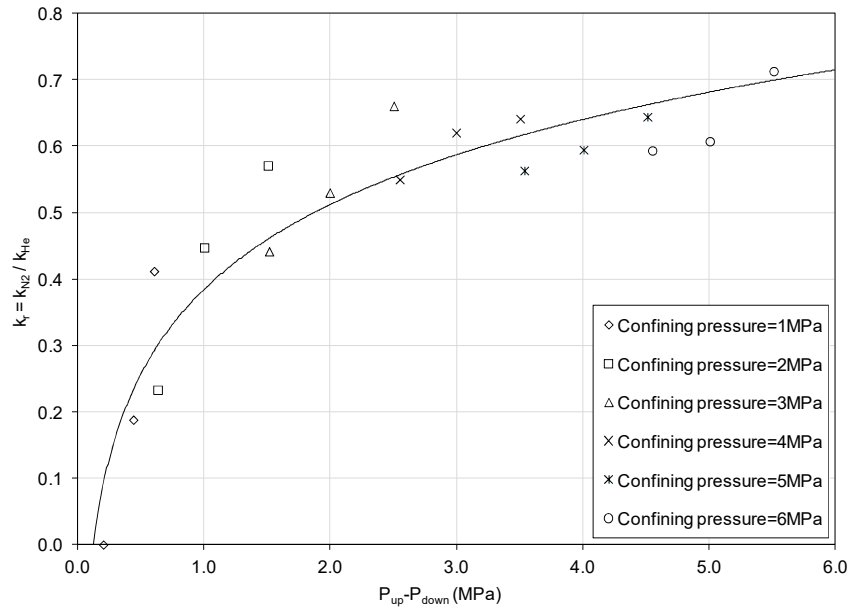


Figure 5c. Variations of the relative permeability (k_r) of the coal sample to N_2 with differential gas pressure at various confining pressures ($T=298\text{K}$).

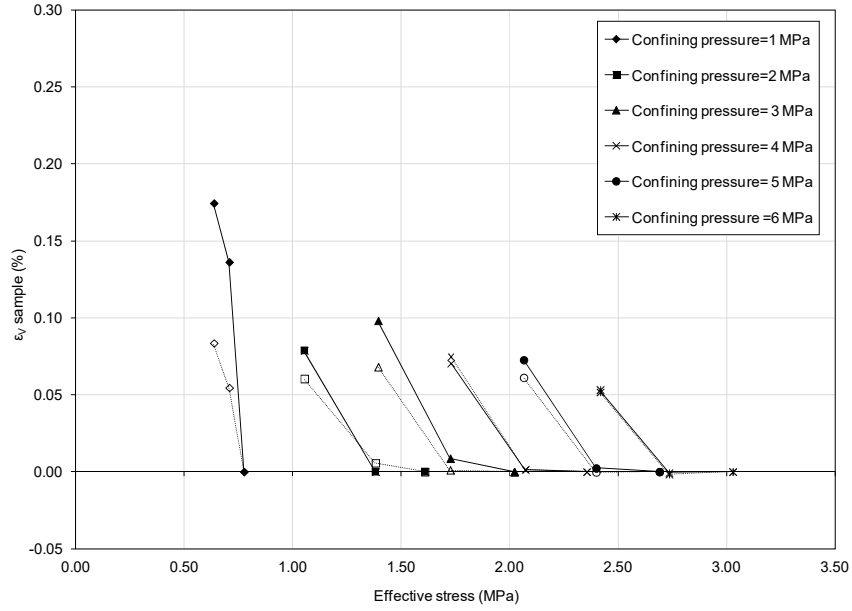


Figure 5d. Variations of volumetric expansion of the coal sample versus effective stress variations due to increase in N₂ pressure at constant confining pressures (T=298K); (dashed lines show the volumetric expansions of the coal sample during phase 1 of helium flooding experiment).

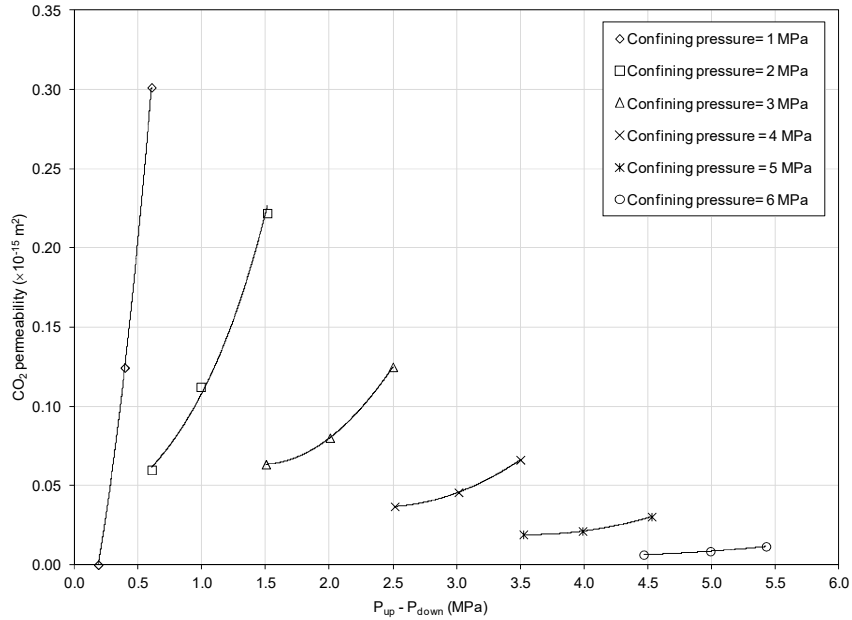


Figure 6a. Variations of permeability of the coal sample to CO₂ versus differential gas pressure at various confining pressures (T=298K).

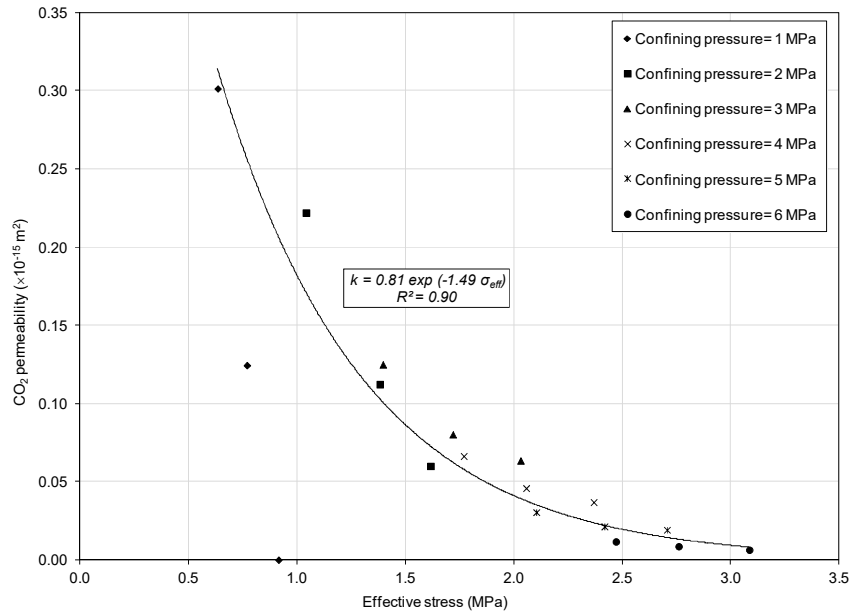


Figure 6b. The relationship between permeability of coal to CO₂ and effective stress (T=298K).

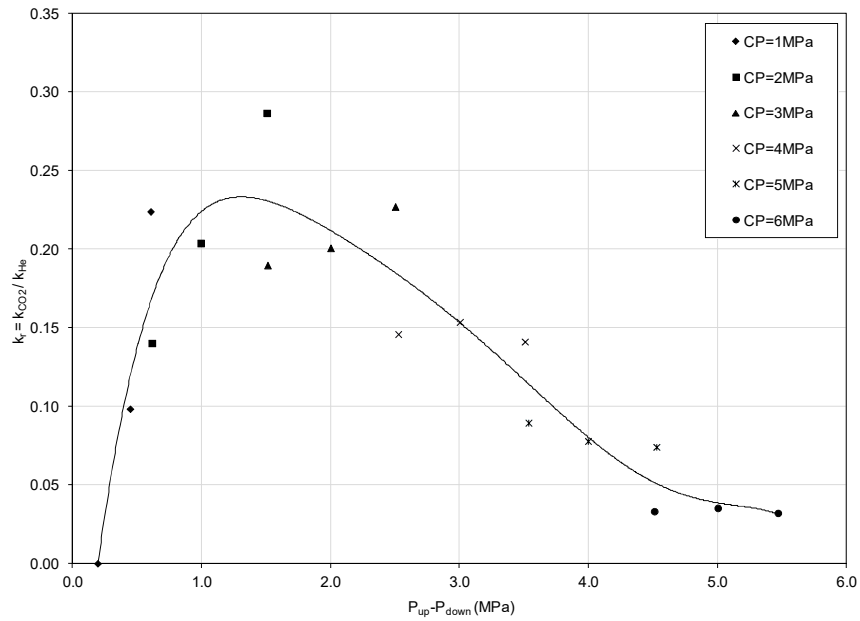


Figure 6c. Variations of the relative permeability (k_r) of the coal sample to CO₂ with differential gas pressure at various confining pressures (T=298K).

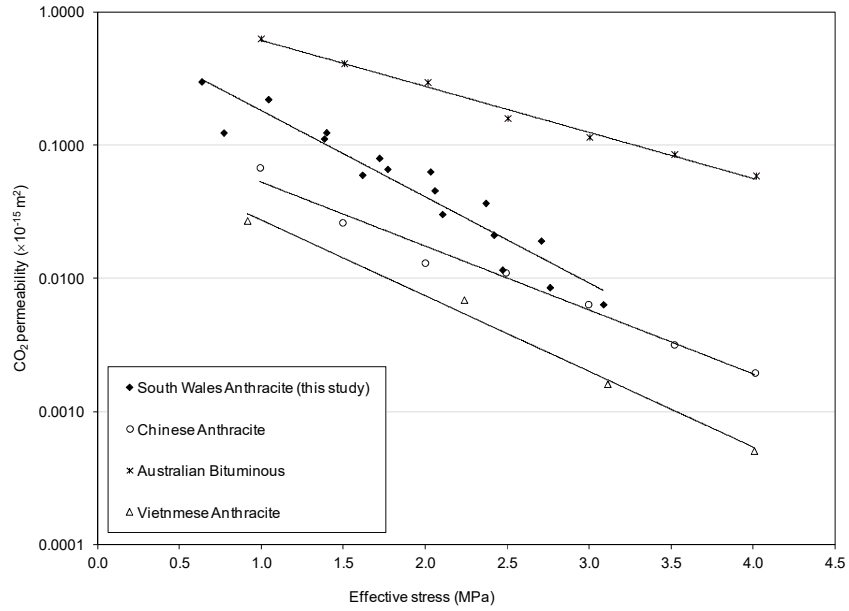


Figure 6d. CO₂ permeability evolution with effective stress for the coal sample of this study (South Wales Anthracite) and other types of coal studied by Huy et al. (2010).

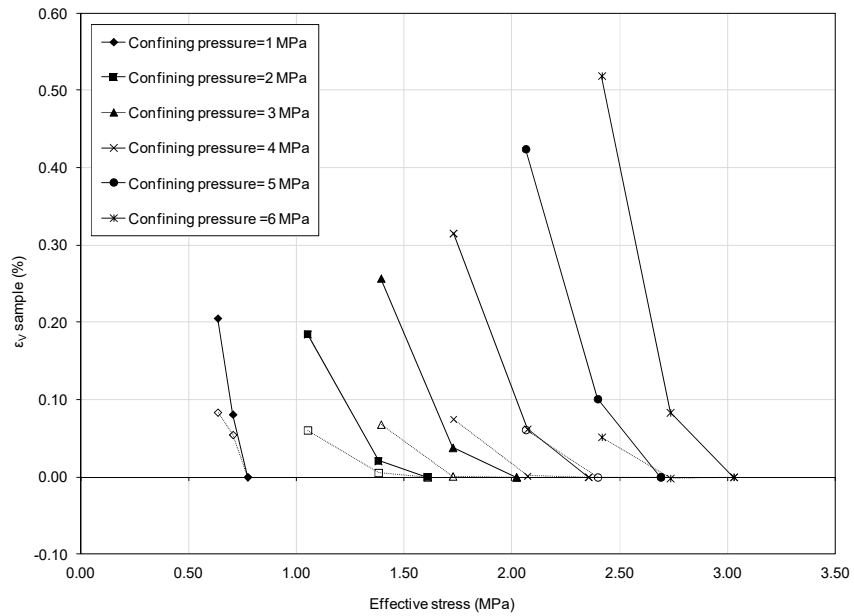


Figure 6e. Variations of the volumetric expansion of the coal sample with effective stress variations due to increase in CO₂ pressure at constant confining pressures (T=298K); (dashed lines show the volumetric expansions of the coal sample during phase 1 of helium flooding experiment).

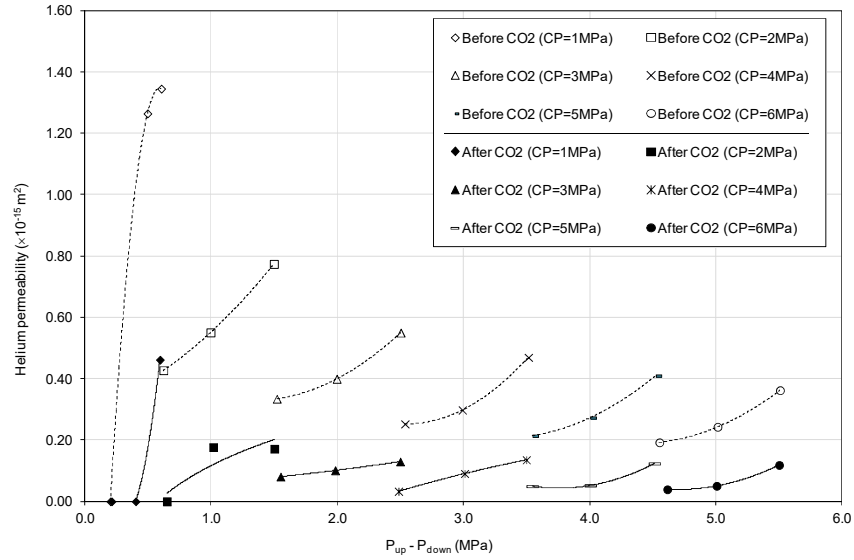


Figure 7a. Variations of the helium permeability of the coal sample with differential gas pressure before (dashed line) and after (solid line) CO₂ injections (T=298K).

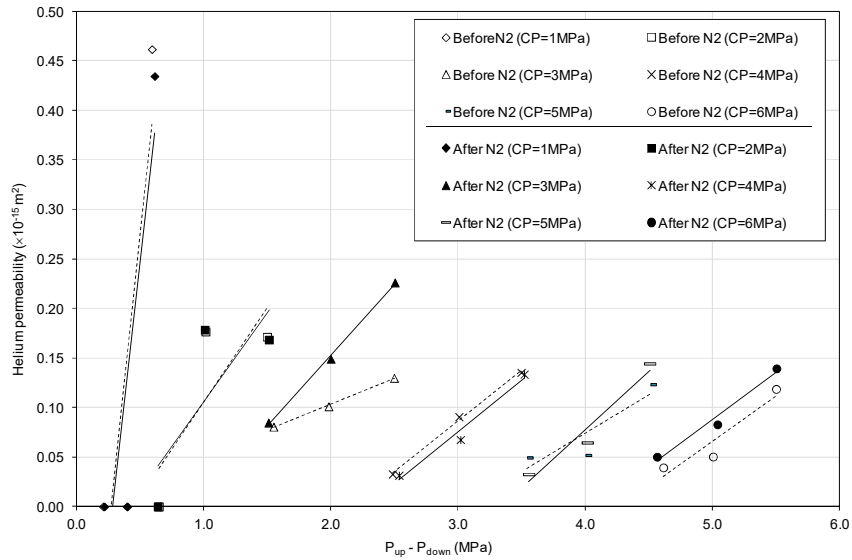


Figure 7b. Variations of the helium permeability of the coal sample with differential gas pressure before (dashed line) and after (solid line) the phase 2 of N₂ injections (T=298K).

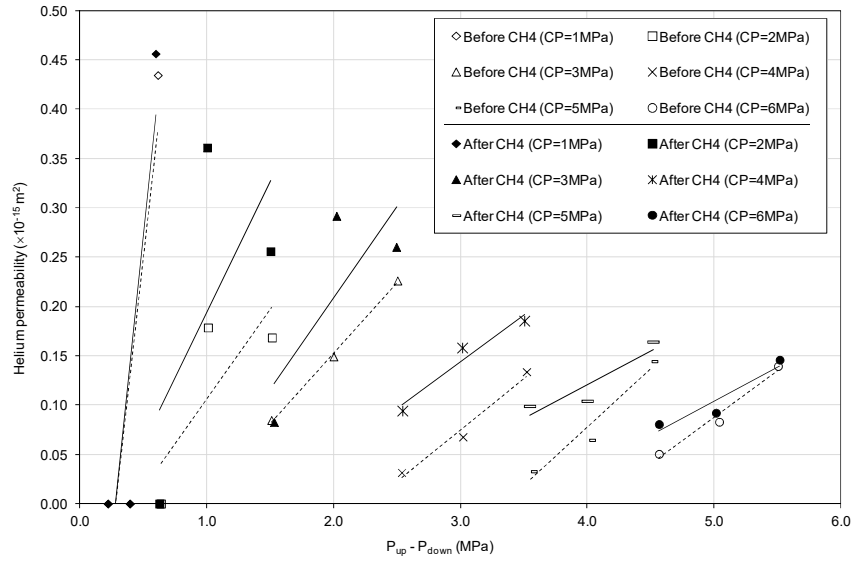


Figure 7c. Variations of the helium permeability of the coal sample with differential gas pressure before (dashed line) and after (solid line) the CH₄ injections (T=298K).